Bioactive Materials 22 (2023) 225–238

Contents lists available at ScienceDirect

Bioactive Materials

journal homepage: www.keaipublishing.com/en/journals/bioactive-materials

A biodegradable magnesium surgical staple for colonic anastomosis: *In vitro* and *in vivo* evaluation

Yue Zhang [a,b,1], Jian Cao [c,1], Mengmeng Lu [d], Yi Shao [a,b], Kewei Jiang [c], Xiaodong Yang [c], Xiaoyu Xiong [c], Shan Wang [c], Chenglin Chu [a], Feng Xue [a,b], Yingjiang Ye [c,**], Jing Bai [a,b,e,*]

[a] Jiangsu Key Laboratory for Advanced Metallic Materials, School of Materials Science and Engineering, Southeast University, Nanjing, 211189, China
[b] Institute of Biomedical Devices (Suzhou), Southeast University, Suzhou, 215163, China
[c] Department of Gastroenterological Surgery, Peking University People's Hospital, Beijing, 100044, China
[d] Department of Oral Implantology, The Affiliated Stomatological Hospital of Nanjing Medical University, Nanjing, 210029, China
[e] Jiangsu Key Laboratory for Light Metal Alloys, Nanjing, 211212, China

ARTICLE INFO

Keywords:
Gastrointestinal tract
Degradation
Bursting pressure
Anastomotic stoma
Colon reconstruction

ABSTRACT

Staplers have been widely used in the clinical treatment of gastrointestinal reconstruction. However, the current titanium (Ti) staple will remain in the human body permanently, resulting in some adverse effects. In this study, we developed a type of biodegradable staple for colonic anastomosis using 0.3 mm diameter magnesium (Mg) alloy wires. The wire surface was modified by micro-arc oxidation treatment (MAO) and then coated with poly-L-lactic acid (PLLA) to achieve a moderate degradation rate matching the tissue healing process. The results of tensile tests on isolated porcine colon tissue anastomosed by Mg and Ti staples showed that the anastomotic property of Mg staples was almost equal to that of Ti staples. The *in vitro* degradation tests indicated the dual-layer coating effectively enhanced the corrosion resistance and maintained the tensile force of the coated staple stable after 14-day immersion in the simulated colonic fluid (SCF). Furthermore, 24 beagle dogs were employed to conduct a comparison experiment using Mg-based and clinical Ti staples for 90-day implantation by ent-to-side anastomosis of the colon. The integrated structure of Mg-based staples was observed after 7 days and completely degraded after 90 days. All animals did not have anastomotic leakage and stenosis, and 12 dogs with Mg-based staples fully recovered after 90 days without differences in visceral ion levels and other side effects. The favorable performance makes this Mg-based anastomotic staple an ideal candidate for colon reconstruction.

1. Introduction

Since the 1980s, an increasing number of anastomotic devices have been used in clinical surgery [1]. Compared with manual suture, the application of anastomotic staples shortens the operation time, reduces surgical complication, and alleviate the patient's pain [2]. With the increase of digestive tract cancer patients and gastric bypass surgeries [3], anastomotic devices come higher growth. However, current titanium (Ti) staples cannot be absorbed and remain in the human body permanently, which may affect the medical image observation during follow-up surveys and elicit local inflammation and other complications [4–6]. In recent years, biodegradable materials attract much attention in the field of medical implants [7]. Although biodegradable surgical sutures made by polymers, such as polydioxanone, polylactic, and polyglycolic acid, have been applied in clinical practice [8–10], surgical staples are still titanium staples due to the lack of suitable biodegradable metal materials.

To date, iron, zinc, magnesium (Mg), and their alloys as promising biodegradable metallic materials have been attracting much attention from researchers for more than a decade [7,11–13]. Numerous efforts have been devoted to evaluating their mechanical, degradation, and biological properties. A perfect degradation time of implants matching

Peer review under responsibility of KeAi Communications Co., Ltd.
* Corresponding author. Jiangsu Key Laboratory for Advanced Metallic Materials, School of Materials Science and Engineering, Southeast University, Nanjing, 211189, China.
** Corresponding author.
E-mail addresses: yeyingjiang@pkuph.edu.cn (Y. Ye), baijing@seu.edu.cn (J. Bai).
[1] Yue Zhang and Jian Cao have contributed equally to the work.

https://doi.org/10.1016/j.bioactmat.2022.09.023
Received 27 April 2022; Received in revised form 3 September 2022; Accepted 21 September 2022

the tissue healing is the most desired ambition in any application environment. However, although iron and zinc-based materials have better mechanical properties than Mg, their low degradation rate does not have the advantage for intestinal tissue healing. Guo et al. [14] implanted the zinc alloy for gastrointestinal anastomosis, and the degradation rate of the zinc alloy is so slow that it remained nearly intact after 12 weeks. Besides, the aging and creep of zinc alloys at room temperature are still unsolved obstacles for applications. As for the iron alloys, besides the lower degradation rate, the stable iron hydroxides are also hard to be eliminated by the body, possibly inducing the local tissue reaction [15,16]. Therefore, although the rapid degradation rate of Mg alloys limits their applications for long-term implantation, they may be more suitable for intestinal remodeling, especially with the development of coating technology in recent years.

The earliest attempt to use Mg alloys in gastrointestinal anastomosis occurred in 1907. Chlumsk'y [7] implanted a tubal Mg connector in the dog's stomach and intestine, showing the preliminary feasibility of Mg application in the gastrointestinal tract. Nevertheless, the time of effective support and entire disintegration strongly depend on the anatomical location and the size of the implant. Thus, only 0.3 mm of the clinical Ti staple diameter brings a challenge between the tissue joining with the degradation time of devices if we use Mg alloys instead. Recently, with the improvement of Mg alloy processing technology, using Mg alloys in the gastrointestinal tract has attracted attention again [17–19]. Implanting the Mg–6Zn (wt.%) pins in Sprague-Dawley rats' cecum and the high-Purity magnesium (HP–Mg) staples in transgenic mice rectal demonstrated the Mg degradation could suppress the inflammatory response compared to the medical Ti alloy [20–22]. Wu et al. [2] also put the high purity magnesium staples for the lateral closure of the stomach in three pigs. However, the current studies on biodegradable Mg staples are still insufficient. On the one hand, unlike the body fluid and blood environment, the gastrointestinal tract belongs to the external environment of the human body. Its internal environment varies with the different digestive functions of each part, including the pH value, ion balance, enzymes, and so on [13,14,17,18]. Moreover, the anastomotic approach also affects the service environment of the implanted staple. For example, end-to-side or end-to-end anastomosis exposes the anastomotic stoma into the internal environment of the gastrointestinal tract, whereas the end closure of the gastric or intestine may result in the isolation of the staple from the gastric or intestinal fluid. These differences in the physiological environment can greatly affect the degradation of staples. On the other hand, due to the standardization of stapler specifications for clinical use, the current stapler used in humans is not suitable for the stomach and intestine of small animals, such as rabbits, and mice. This leads to the need for large animal experiments to verify the feasibility of staples *in vivo*. Therefore, up to now, there is still a lack of a systematic evaluation of Mg staples including the *in vitro* test, the tissue healing, physiological indicators, and the entire degradation time, especially for colonic anastomosis.

For intestinal anastomosis, the first week after surgery is critical for patients, because the anastomotic stoma needs adequate support from staples during this period. In this work, considering the effects of the intestinal fluid and the dynamic loadings caused by the intestinal peristalsis on the degradation of staples [23,24], we prepared a full-biodegradable Mg-based surgical staple with a dual-layer coating including micro-arc oxidation treatment (MAO) layer and poly-L-lactic acid (PLLA) layer to acquire a moderate degradation rate in agreement with the healing time. To explore the application potential of this Mg-based staple, we conducted elaborate *in vitro* work and *in vivo* implantation experiments to evaluate its long-term safety, efficacy, and degradation behavior. More importantly, 24 beagle dogs were employed to ensure the statistical significance of the data. In addition, since we completed all animal experiments in 2012, more than ten years had passed. Due to the lack of research on medical magnesium alloys at that time, AZ31 alloy with good strength and plasticity but containing Al was selected as the material for making staples. This has been improved in our subsequent studies, with our in-depth research on the preparation technology of magnesium alloy wires [17,18,25,26]. To date, even though some progress has been made in the application of magnesium alloys in the gastrointestinal tract, people still lack confidence in magnesium alloys as anastomotic staples, especially in their mechanical properties, due to the lack of a large number of reports on large animal experiments. Therefore, we hope that this study can provide some helpful theoretical support for the development and application of magnesium alloys in gastrointestinal anastomosis.

2. Materials and methods

2.1. Materials and preparation

AZ31 alloy (wt.%, the chemical composition is shown in Table S1) wires with a diameter of 0.3 mm were prepared through our extrusion and cold-drawing technologies. The wire shows very good comprehensive mechanical properties with 302 ± 4 MPa in tensile strength and above 23 ± 3% in breaking elongation, which is higher than the requirement regulated by the Medical industry standard of China YY 0875–2013. The wire was firstly treated by the MAO method in the alkaline electrolyte solution containing Na_2SiO_3 of 13 g/L, Na_3PO_4 of 5 g/L, and NaOH of 2.5 g/L at a current density of 0.56 A/m with the Mg wire as the working electrode and stainless steel as the counter electrode. The frequency was 500 Hz, and the duty factor was 15%. The operation under the direct constant current mode should be stopped while the working voltage was up to 280 V. All wires were washed with deionized water three times and dried at room temperature for 12 h. The thickness of the prepared MAO coating is about 2 μm. To obtain the dual-layer coating, Mg wires with the MAO coating were soaked into the PLLA solution for 20 min and lifted out vertically at the speed of 2 cm/s. The medical-grade PLLA (Jinan Daigang Biological Engineering Co., Ltd. China) with a weight average molecular weight of 400,000 g/mol was weighed in the desired proportions and dissolved in the dichloride solution to obtain a 20% (w/v) solution. The dip-coating from the PLLA solution was done once and dried at room temperature for 24 h. The diameter of the wire with the PLLA coating is between 0.33 mm and 0.35 mm. Fig. 1(a) depicts the schematic illustration of the coatings' fabrication process and the cross-section of the wire with the MAO and PLLA coating (MP).

Afterward, these Mg-MP wires were winded around a trapezoidal mold designed according to the clinically used U-shaped titanium staples, and the long side of the trapezoidal mold was removed using a file. Fig. 1(b) shows the morphology of the U-shaped staple and B-shaped staple molded by a stapler and illustrates images of Mg staples nailed on the isolated pig colon tissue.

2.2. In vitro studies

2.2.1. Cytocompatibility evaluation

The evaluation of cell viability was conducted according to ASTM 10993–5:2009. Murine fibroblast cells (L-929) and intestinal epithelial cells (IEC-6) were utilized and cultured in Eagle's Minimum Essential Medium (EMEM) and Dulbecco's Modified Eagle's Medium (DMEM) supplemented with 10% fetal bovine serum (FBS), 100U/ml penicillin, and 100 μg/ml streptomycin at 37 °C in a humidified atmosphere of 5% CO_2, respectively. The extracts of three kinds of staples were obtained by incubating staples with an extraction ratio of 1.25 cm^2/ml in the above culture medium for 24 h, and the supernatants were collected. After that, cells were incubated in 96 - well culture plates at a density of 3 × 10^3 cells/well for 24 h to allow cell attachment. Then the medium was replaced by extracts of staples except for one group as a negative control. After incubating for 1, 4, and 7 days, the cell viability was detected using the Alarmar Blue Kit (Merck, Germany). The spectrophotometric absorbance of each well was measured with a microplate reader (MultiskanGO, Thermo, USA) at 570 nm wavelength and 600 nm

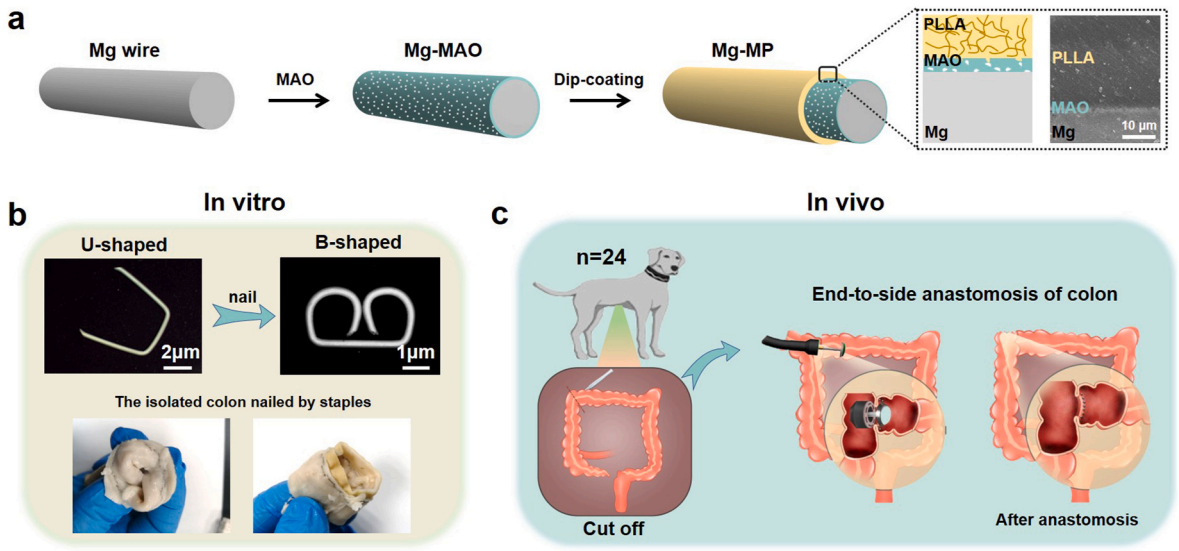

Fig. 1. Schematic illustration of coatings' fabrication process and the cross-section of the Mg-MP wire (a). Morphologies of the U-shaped and B-shaped staple and images of Mg staples nailed on the isolated pig colon tissue by a tubular cutter stapler (b). The schematic diagram of colonic end-to-side anastomosis (c).

wavelength, respectively. To evaluate the influence of extracts on cell morphologies, cells were washed with phosphate buffer solution (PBS) and fixed in 4% paraformaldehyde for 10 min at room temperature. 0.1% Triton was added and reacted for 7 min. Finally, 5 μg/ml FITC-phalloidin dye was added and incubated for 30 min, and the cell nuclei were stained by DAPI dye. Cell morphologies were visualized using an Inverted fluorescence Microscope (IX83, Olympus, Japan).

2.2.2. Hemolysis test

The fresh blood from healthy rabbits containing sodium citrate (3.8 wt%) in the ratio of 9:1 was taken and diluted with the normal saline (NS, 4:5 ratio by volume). The extract of Mg-MP staples was obtained by incubating staples with an extraction ratio of 1.25 cm^2/ml in the normal saline and Hanks' solution (Hanks') at 37 °C for 1, 2, and 3 days, referring to the standard ISO 10993–12:2012. The normal saline and Hanks' solution were used as negative control groups and the deionized water as the positive control group. After that, 0.2 ml of diluted blood was added to extracts and control groups, and these mixtures were incubated for 60 min at 37 °C. Finally, all mixtures were centrifuged for 5 min at 3000 rpm, and the supernatant was transferred to the 96 - well plates for spectroscopic analysis at 545 nm using the microplate reader.

2.2.3. Intestinal anastomosis test

To evaluate the anastomosis properties, the bursting pressure test and the tensile test were conducted on the colon tissue anastomosed by staples. For the bursting pressure test, the isolated tissue was firstly cut into two pieces and anastomosed end-to-end by a tubular stapler equipped with twenty surgical staples. Then, the colon was filled with water after being connected with a pressure detecting device. This measurement was repeated 3 times [27]. Moreover, the tensile test was carried out on the intestine anastomosed by a tubular stapler equipped with twenty staples and by a linear stapler equipped with nine staples. The tensile test was measured employing a static testing system (Zwick/Roell, Germany) at room temperature with a speed of 2 mm/min until specimens failed.

2.2.4. Immersion test

The degradation behavior was characterized by immersion tests in simulated colon fluid (SCF) prepared according to 2015 Chinese pharmacopeia. The simulated colon fluid was obtained by dissolving 6.804 g/L KH_2PO_4 and 1.696 g/L NaOH in distilled water and adjusting the pH to 7.6 by 0.2 mol/L NaOH solution. All the immersion containers were kept at (37.5 ± 0.5) °C, in the atmosphere (mainly 21% O_2, 0.03% CO_2). Staples were hung into the solution using a nylon thread. The ratio of the solution volume to the specimen area was 10 ml/cm^2 in terms of the ASTM-G31-72 standard, and the immersion media was refreshed every day. Samples were removed from the solution after 7, 14, 21, and 42 days, gently rinsed with distilled water, and dried in air for weighting and observation. To further simulate the degradation in the body, staples nailed on the simulated intestinal material were also immersed in SCF with the ratio of the solution volume to the specimen area of 10 ml/cm^2. Samples were removed from the solution after 14 and 28 days for observation by 3D X-ray microscopy (XRM, Zeiss Xradia 510Versa, Germany). The degradation morphology was observed by Sirion200 Field Emission Scanning Electron Microscope (FE-SEM, FEI, USA). The soluble magnesium ions were measured using an inductively coupled plasma emission spectrometer (ICP, SPECTROBLUE ICP-OES, Germany).

2.2.5. Tensile force of the single staple

To evaluate the mechanical property of a single staple, we conducted the tensile test on Mg staples after the immersion of 7 and 14 days. The staple, which involved passing a nylon thread through each loop of the B-shaped, was strained by the universal testing machine at a strain rate of 2 mm/min until fracture (Fig. S1).

2.2.6. Electrochemical measurements

To test the actual electrochemical behavior of samples, half a staple was immersed in the solution as the working electrode. The saturated calomel electrode (SCE) was as a reference electrode, and a platinum mesh was as a counter electrode. The electrochemical impedance measurement (EIS) was conducted in an electrochemical system (PARSTAT 3000A, AMETEK, USA) and performed at the frequency from 100 kHz to 10 mHz at the OCP value with an AC amplitude of 5 mV. All electrochemical experiments were carried out using a quartz cell at (37.5 ± 0.5) °C, in the atmosphere (mainly 21% O_2, 0.03% CO_2). Three parallel tests were conducted for different samples.

2.3. In vivo animal surgery

2.3.1. Surgical implantation

The animal experimental protocol was authorized by the medical ethics committee of Peking University People's Hospital according to the Guidance Suggestions. Animals were fed by the Laboratory Animal Science Department of Peking University Health Science Center. 24

beagle dogs with a weight of 9–11 kg were randomized into two groups (Mg-MP staples as an experimental group and Ti staples as a control group) for colonic anastomosis. Dogs were sacrificed for observation at postoperative 7 days (6 dogs) and 90 days (18 dogs). All surgical operations were performed through the blinding method by the same skilled general surgeons.

Preoperative fasting and fasting water were at 12 h and 6 h before surgery, respectively. Dogs were placed in the supine position with the trachea cannula and limbs fixed, as shown in Fig. S2(a). The surgery was performed after establishing venous access and injecting pentobarbital sodium (25–30 ml/kg), then dogs were assigned to receive colonic end-to-side anastomosis. Firstly, the colon was cut off at a 20 cm distance from the cecum. The tubular stapler anvil was put into the distal colon , and the main body of the stapler speared the wall of the proximal colon. Fig. 1(c) illustrates the schematic diagram of colonic end-to-side anastomosis, and Fig. S2(b) shows the process of using the stapler. After that, the residual port was closed with the purse-string suture, and hemostasis was conducted immediately after closure. Finally, the abdominal incision was sutured layer by layer. All animals received an intramuscular injection of four hundred thousand units of penicillin to prevent infection every 12 h for the first 3 days.

2.3.2. Intestinal healing test

To investigate wound healing, we conducted the bursting pressure test at postoperative 7 days and 90 days and recorded the rupture position meanwhile. The pressure value was collected when the water overflowed. Before testing anastomotic pressure, the pH value of fluid surrounding the staples was measured firstly by pH test strips.

2.3.3. Computed tomographic examination

Computed tomographic scanning was performed after 7 days and 90 days to analyze the *in vivo* degradation of Mg-MP staples by 64 - row spiral computed tomographic equipment (CT, GE, USA) from the diaphragmatic apex to the rectal plane. Dogs had been fasting 24 h before the examination. The X-ray tube was set at 120–140 kV and 140–220 mA with a scan layer thickness of 5 mm. The scanning results were reconstructed and analyzed by two radiologists blindly.

2.3.4. Histology evaluation

The colon segments with staples at postoperative 7 days and 90 days were divided into two groups. One group was fixed in 10% neutral buffered formalin for 48 h and then sectioned at 4 μm thickness. Histological samples were processed and stained with hematoxylin-eosin (H&E), Masson staining, and Sirius picric acid. Another group performed immunohistochemistry with the anti - CD3, anti - CD20, and anti - CD68. All images were blind-assessed by a senior pathologist to estimate the difference between Mg and Ti groups.

2.3.5. Physiological indexes detection of animals' blood and inner organs

Dogs' peripheral blood collected at preoperative 1 day and postoperative 7, 28, and 90 days was detected by an automatic blood cell analyzer (LH750, Beckman Coulter, USA), including hemoglobin (Hb), leukocyte (WBC), and platelet (PLT). The centrifugal blood serum was detected by an automatic biochemical analyzer (LST008, Hitachi, Japan), including alanine aminotransferase (ALT), aspartate aminotransferase (AST), albumin (ABL), urea nitrogen (BUN), creatinine (Cr), magnesium ion, calcium ion, potassium ion. The detection of magnesium, aluminum, zinc, and manganese in the heart, liver, kidney, liver, brain, spleen, and skeletal muscle were analyzed by an inductively coupled plasma mass spectrometer (DRC-II, PerkinElmer, USA) and a plasma emission spectrometer (iCap6000, Thermo Fisher Scientific, USA).

2.3.6. Ultrastructure of tissue

The ultrastructure of intestinal epithelium tissue and organ slices from the heart, kidney, liver, spleen, and brain were observed by the Tecnai G2 transmission electron microscope (TEM, FEI, USA). Briefly, tissue specimens were firstly fixed in 1.5–3% glutaraldehyde for 2 h and washed with PBS thrice. And then, samples were fixed in osmic acid, washed by PBS twice, and subsequently dehydrated stepwise in gradient ethanol. Finally, they soaked in a mixture of ethanol and epoxypropane for 10 min, inlaid in resin, and cut into slices. Slices were stained with uranium for 15 min and lead for 10 min.

2.4. Statistical analysis

Statistical analysis was performed with the SPSS 17.0 software package (SPSS Inc., Chicago, USA). Using the mean values ± standard deviation (*SD*) presented the experimental data. One-way analysis of variance (ANOVA) followed by the least significance difference (LSD) posthoc test was used for statistical analysis among groups *in vitro*. The independent sample *t*-test was carried out on the data between the two material groups at each time point *in vivo*. The statistical difference was defined as $p < 0.05$.

3. Results

3.1. In vitro results

3.1.1. In vitro biocompatibility

Fig. 2(a) shows cell morphologies of L-929 and IEC-6 cultured in the extraction mediums for 4 days, and their viabilities after 1, 4, and 7 days of culture are depicted in Fig. 2(b and c). In all groups, the cell grows densely with normal adherence and uniform distribution. The shape of the L-929 cell is round or polygonal, and that of the IEC–6 cell is fusiform or polygonal. Cells' cytoskeletal structure is not affected after using extracts, and their viabilities are higher than 85%, indicating that the three staples have excellent cytocompatibility. Thus, the degradation of Mg-MP staples shows no significant cytotoxicity.

Fig. 2(d) displays the hemolysis caused by the extraction medium of Mg-MP staples at different time points. It can be found that there was no obvious hemolysis reaction in both solutions. Fig. 2(e) lists the pH value of the extraction medium after the immersion for 3 days, and the pH value of normal saline and Hanks' solution are 10.4 ± 0.3 and 8.7 ± 0.3, respectively. The increase in pH value is attributed to the degradation of the staple's tip which is not protected by coatings. However, due to the slow degradation of the whole staple, the corresponding hemolysis ratio is less than 2%. The degradation of Mg-MP staple can meet the requirement of hemolysis for implants. Additionally, the skin sensitization test and intracutaneous stimulation test are conducted by following the standard ISO 10993–10: 2010, as shown in Fig. S3, and the corresponding record of the skin reaction is listed in Table S2 and Table S3, respectively. It can be seen that there is no evidence of delayed-type skin sensitization and stimulation caused by the biodegradable Mg-MP surgical staples.

3.1.2. Intestinal anastomosis properties

Fig. 2(f) shows the isolated intestine nailed by the tubular and linear stapler employing Mg staples. After the manufacturing process, the intestines are tightly connected without staples damaged or abnormally deformed. Fig. S4 depicts the intestine anastomosed by Mg staples filled with water. There is no leakage when the bursting pressure is about 3.6 kPa which is regulated by general technical conditions for a stapler in YY0245-2008. This indicates that the magnesium alloy surgical staple can provide sufficient mechanical support after anastomosis. To characterize the damaging behavior of the intestine after anastomosis, the uniaxial tension test was conducted. The maximum bearable force of the intestine nailed by Mg staples is slightly lower than that nailed by Ti staples when the intestine is anastomosed using a tubular stapler (Fig. 2(g), Fig. S5), but it is not statistically significant. As for linear anastomosis, the maximum bearable force of the intestine nailed by Mg and Ti staples is almost equal to each other. Moreover, all the broken positions

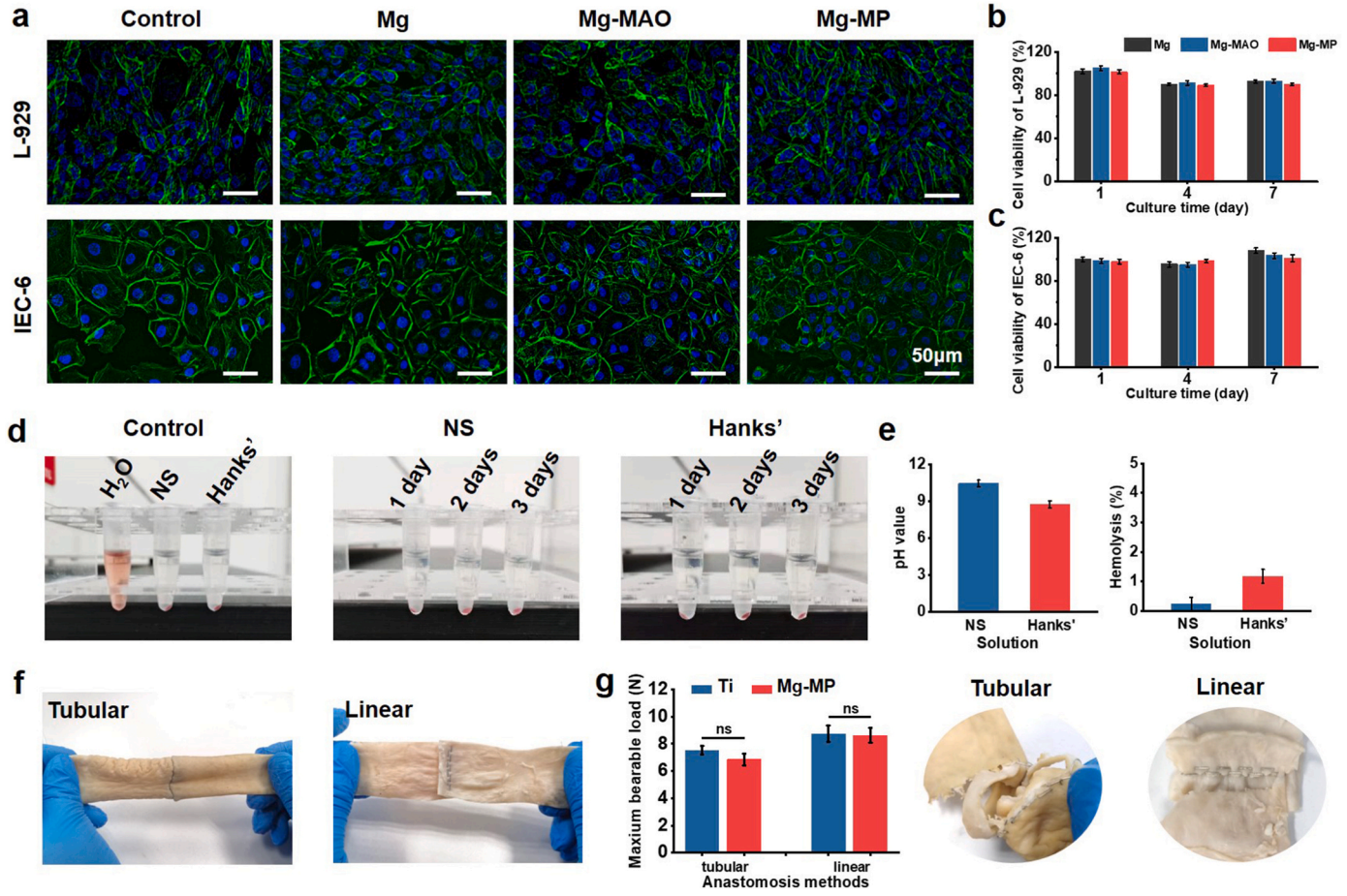

Fig. 2. Fluorescent morphologies of L-929 and IEC-6 cells cultured in the extracts of Mg, Mg-MAO, and Mg-MP staples after 4 days (a), and the cell viability expressed as a percentage of the viability after 1, 4, and 7 days of culture (b) and (c). Photographs of hemolysis caused by the extraction medium of Mg-MP staples at a different time (d). The pH value of extracts after incubating Mg-MP staples for 3 days and the corresponding hemolysis ratio (e). Images of isolated porcine colon tissue anastomosed using Mg staples by the tubular stapler and linear stapler (f). The maximum bearable load of the intestine anastomosed by Mg and Ti staples and images of broken position after tensile tests (g).

are at the anastomotic sites, and a neat fracture is found at the nail hole within both groups. Mg staples exhibit good performance for intestinal anastomosis *in vitro*.

3.1.3. Degradation properties

The degradation behavior of the Mg-MP staple was evaluated by contrast to the bare Mg staple by static immersion in SCF for different time points since the MAO coating without PLLA covered failed after 60 min in SCF (Fig. S6). Fig. S7 and Fig. 3(a) depict morphologies of bare Mg staples and Mg-MP staples with time, respectively. As can be seen, both staples remain intact after 7 days, while the majority of bare Mg staples are corroded after 14 days. Fig. 3(b) shows the result of the residual mass ratio. The mass loss of bare Mg staples is 76.4 ± 5.7% after 14 days, while that of Mg-MP staples is just 8.5 ± 4.3%, and meanwhile, corrosion pits began to appear on the surface of the Mg-MP staple. As the soaking time increases, the corrosion pits on Mg-MP staples become more apparent, and the residual mass ratio is 36.2 ± 4.3% after 42 days. It is noted that the degradation rate of Mg-MP staples becomes faster in the later stage. Moreover, it can be seen that most of the corroded areas are distributed on the outer side of Mg-MP staples. When the wire is transformed to the U-shaped staple and then to the B-shaped staple, coatings on the area with the large deformation sustain the stress. The inner side of the staple sustains the pressure, causing the PLLA coating to bulge and the MAO coating to warp (Fig. S8(a)). The outer side of the staple is boring to the tension, resulting in cracks in the MAO coating (Fig. S8(b)), in which the PLLA coating is also elongated to be thinner and thereby easily permeated by liquid. Although the breakage of MAO coating led to the local rapid corrosion of the inner and outer parts of the staple with only MAO coating, the outer side of the staple should corrode preferentially, because the early corrosion behavior of Mg-MP staples should be more affected by PLLA coating [28,29]. Furthermore, Fig. 3(c) and Fig. S9 show the details of Mg-MP staples in Fig. 3(a). After the immersion of 7 days, some white cracks leading by the effect of tension and hydrolysis appear on the surface of the PLLA coating, corresponding to the corrosion pits as the arrow marks. With the increase in soaking time, cracks propagate more. The profile of staple feet becomes undulating because of the accumulation of corrosion products, and more corrosion pits appear meanwhile. After 42 days, the PLLA coating cracks completely with the severe corrosion of the staple. Additionally, the electrochemical behavior can assist evaluation of the early corrosion resistance (Fig. 3(d)). With the increase in immersion time, the impedance remains stable from 3 days to 7 days, indicating the dual-layer coating can keep the staple to maintain good corrosion resistance in the early stage.

Fig. 3(e) shows the tensile force of the single staple by the tension test. The mechanical change of staples in early degradation is crucial for the safety of implantation. Herein, the endpoint of the steady deformation is considered as the maximal bearing load of the staple. After 7 days, the maximal load of bare Mg staple is 0.7 N. For the staple with coatings, the maximal load can retain at 1.6 N after 14 days. Besides, the Mg ions released during the degradation process are detected within 45 days (Fig. 3(f)). Since the unit of mg is often used to measure the daily

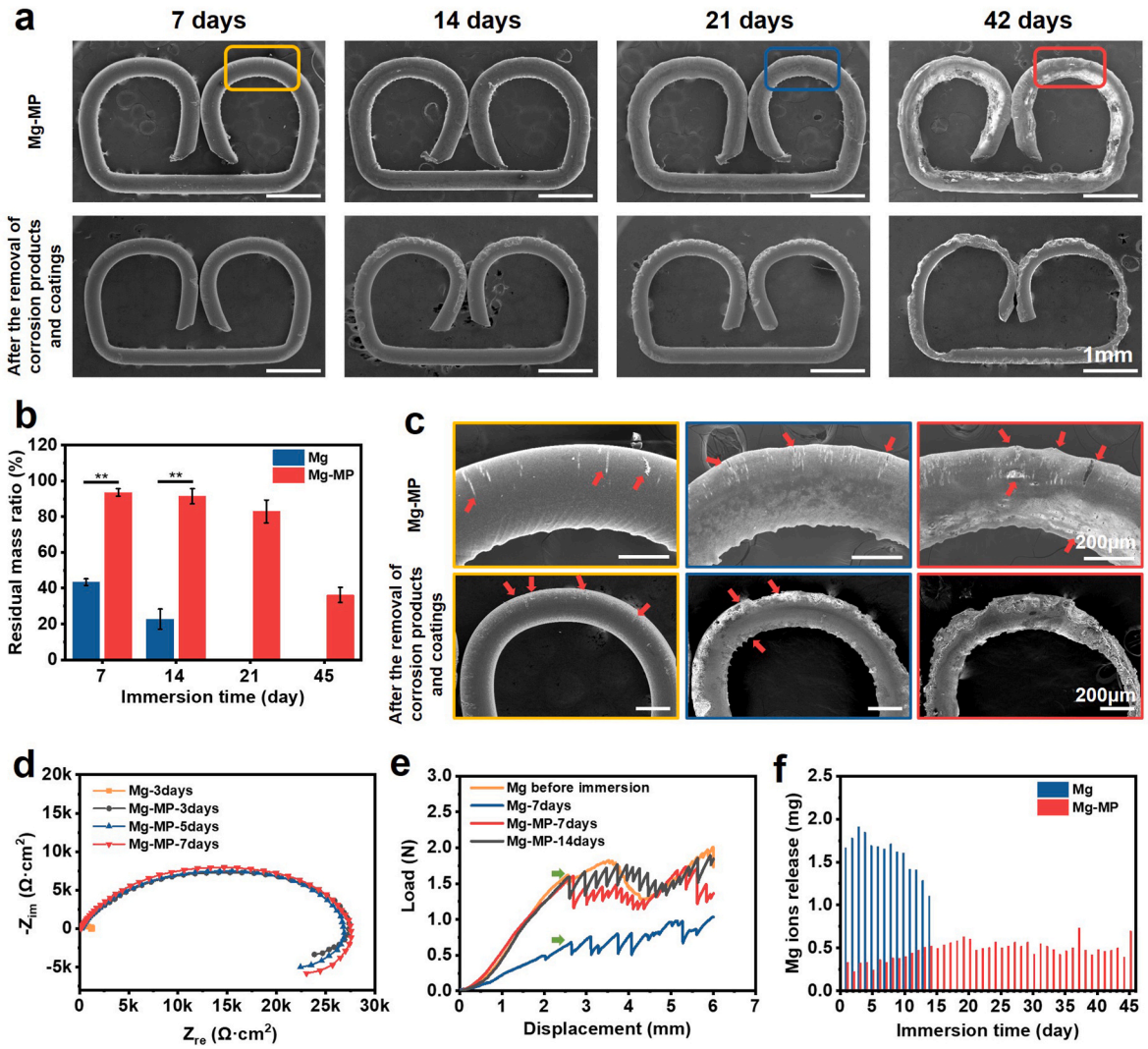

Fig. 3. Morphologies of Mg-MP staples after 7, 14, 21, and 42 days' immersion (a), the residual mass ratio evolution of Mg and Mg-MP staples (**$p < 0.01$) (b), and the details of Mg-MP staples as the area marked in figure (a) by the rectangle (c). Nyquist plots of Mg and Mg-MP staples after immersion (d). The tensile curve of the single staple (e) (the green arrow refers to the endpoint of steady deformation). The weight of magnesium ions released in solution daily (f).

intake, daily soluble ions are calculated based on the solution ion concentration and the number of staples in the tubular stapler. The number of daily magnesium ions released from bare Mg staples and Mg-MP staples is less than 2.2 mg and 0.8 mg, respectively, which is much less than the daily intake amount [30].

To further explore the degradation of staples, staples are nailed on the simulated intestinal material and then immersed in SCF for 28 days. Fig. 4(a) depicts the sample used for the immersion test. It can be seen that Mg staples can hold this material together well without the cross beam and curving feet abnormally deformed. Morphologies detected by XRM after the immersion for 14 days show there is no fracture on staples. The reconstructed image demonstrates that the bare Mg staple is preferred to corrode at the area as green arrows mark, where are not covered by the material. Staples with coatings are no sign of corrosion at this time. When samples are soaked until 28 days, the cross beam and feet of bare Mg staple corrode severely, while the overall structure of the staple is still visible. Meanwhile, small corrosion pits are observed on the Mg-MP staples after 28 days' immersion. The residual mass ratio of bare Mg staples after 28 days is 83.5 ± 0.6%, while only 2.5 ± 0.6% of Mg-MP staples mass is degraded (Fig. 4(c)). The degradation rate of staples nailed on the simulated intestine material is much lower than that of staples by direct immersion. Moreover, the amount of Mg ions released during this degradation process is also lower than that of the human daily intake (Fig. 4(d)).

3.2. *In vivo* results

All beagle dogs survive in good health after surgery. One dog of the control group for the long-term view is not integrated into the following evaluation due to an aspiration event during the postoperative CT examination.

3.2.1. *Postoperative healing situation of animals*

As illustrated in Fig. S10, dogs' weight gradually decreases during the postoperative 7 days due to the dietary control in the first few days after surgery. Signs of weight recovery appear at 28 days. The colon anastomosis fistula and abdominal cavity infection do not happen. A slight adhesion near the anastomotic stoma is found in two groups at 7 days and 90 days (Fig. S11). According to the Knightly grade criteria for abdominal adhesions, Table S4 illustrates the comparison of data statistics. There is no significant difference between the two groups.

CT scanning and dissection test are conducted at postoperative 7 days and 90 days. Fig. 5(a) shows the representative 2D reconstruction images and details of the anastomotic wound. After 7 days *in vivo*, the integrated Ti and Mg-MP staples are detected and observed on the intestinal wall. A part of the surface of the Mg-MP staple has already been

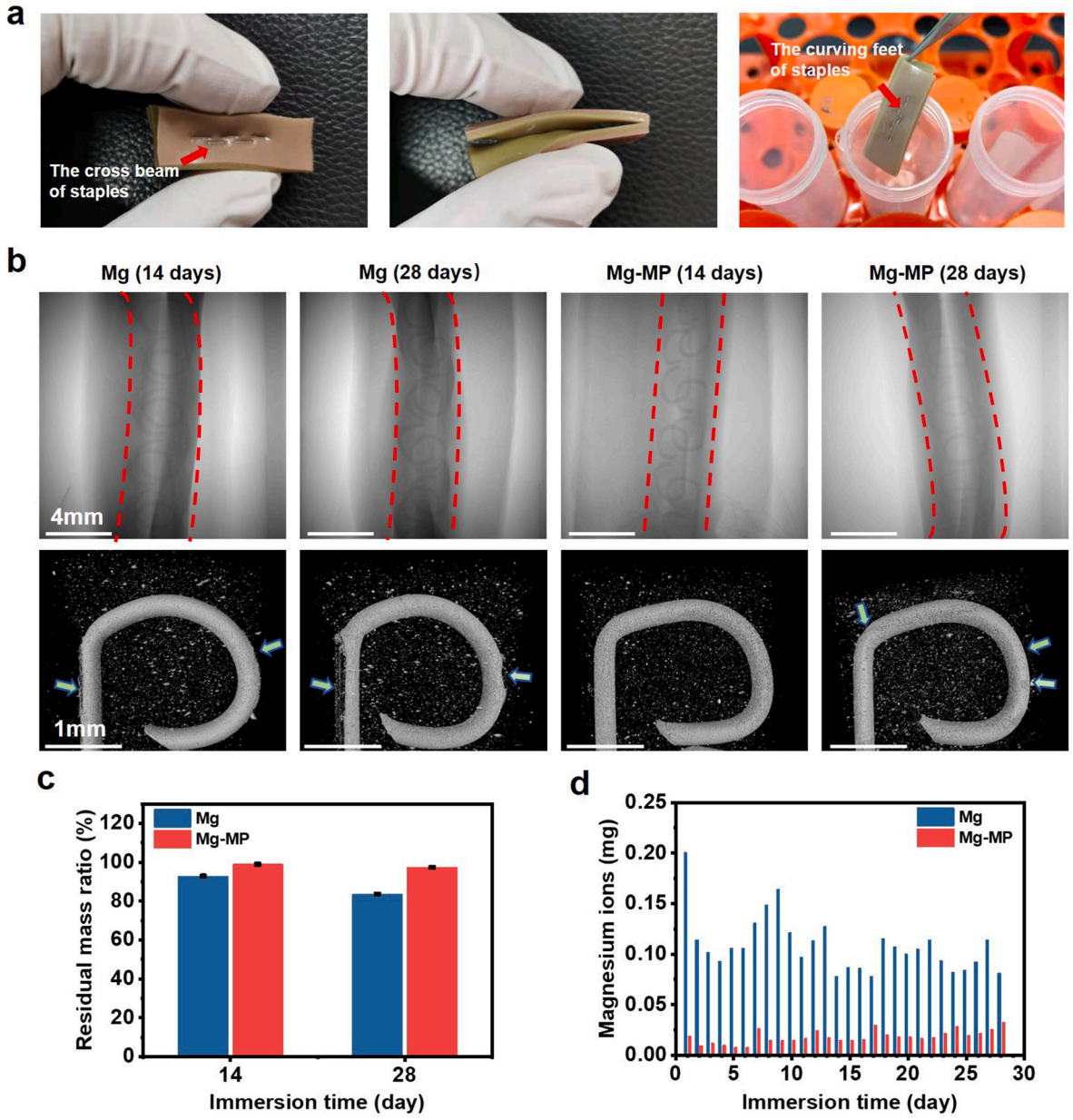

Fig. 4. Images of Mg staples nailing on the simulated intestinal material (a) and morphologies of staples after the immersion of 14 and 28 days (b) (the green arrow refers to the corroded areas). The residual mass ratio of Mg and Mg-MP staples (c) and the number of magnesium ions released (d).

corroded to be dark black, but the part embedded in the tissue is still white. This phenomenon is consistent with the evidence from the *in vitro* immersion. The exposed region to intestinal fluid is degraded initially. At postoperative 90 days, Mg-MP staples are undetected from the CT scanning. From the following dissection observation, Mg-MP staples are degraded completely with the anastomotic wound healed, where the involution of the mucosa and serosa layer is connected neatly and smoothly. In terms of the Ti group, intact Ti staples are seen after 90 days of implantation, and the surrounding intestine tissue is mild swelling.

More importantly, the bursting pressure test is a key to evaluating intestine healing, and the pressure is shown in Fig. 5(b). It can be seen the pressure increases with the implantation time, indicating the tissue is incomplete recovery at postoperative 7 days. The intestine pressure healed with Mg-MP staples after 7 days can be achieved at 27.7 ± 2.5 kPa, nearly 74% of the bearable pressure of healing tissue at 90 days. By contrast, the pressure at postoperative 7 days and 90 days of the Ti staple group are 25.7 ± 4.0 kPa and 35.1 ± 3.8 kPa, respectively. There is no significant difference through data statistics between the two groups, suggesting Mg-MP staples can assume the role of Ti staples for intestine reconstruction. On the other hand, the diameter of the anastomotic stoma is measured as shown in Fig. 5(c), and there is no difference.

Besides, we record the distribution of broken positions after the bursting pressure test and pH value of fluid surrounded staples, as listed in Table 1. The anastomotic stoma connected by staples is prone to rupture after 7 days of implantation. However, broken positions are randomly distributed at the intestinal tube and anastomotic stoma at 90 days. This is assistant evidence to prove that the intestine tissue is not entirely healing at the postoperative 7 days but still has most of the strength of the healthy intestine, which also corresponds to the collagen distribution type around the anastomotic site (Fig. S12). Moreover, the degradation of Mg alloys can lead to the local alkaline areas generally. In this study, the pH value of fluid around the anastomotic stoma in the Mg-MP staple group can remain at 6 to 8. There is no difference compared with the Ti staple group.

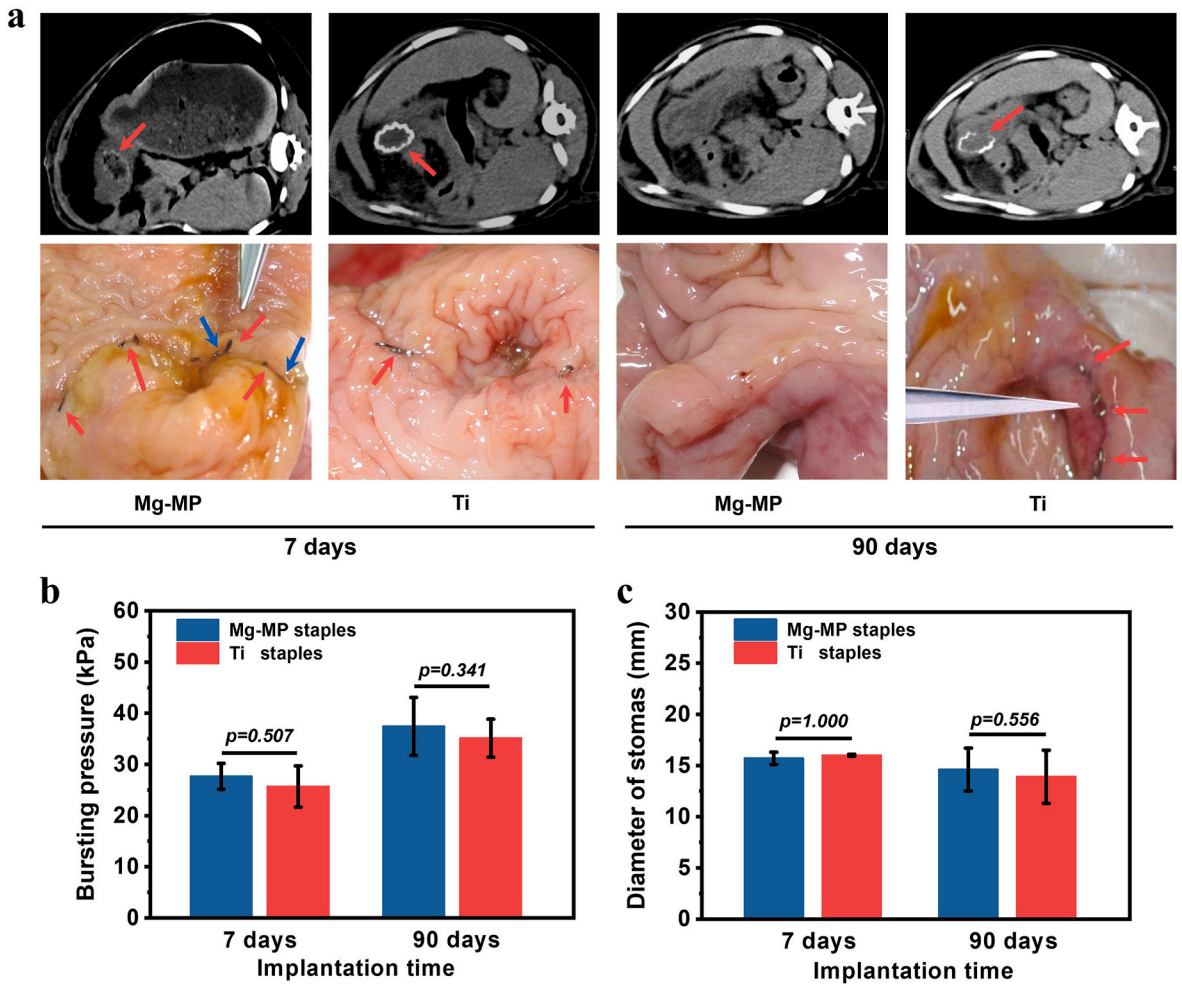

Fig. 5. CT scanning and anatomical observation at postoperative 7 days and 90 days (a) (red arrows show the existence of staples, and blue arrows mark the white surface of Mg-MP staples). The statistic of intestinal bursting pressure (b) and anastomotic stoma diameter within Mg-MP and Ti staple groups at postoperative 7 days and 90 days (c).

Table 1
The statistics of broken positions and the pH value of the fluid surrounding implants during the bursting pressure test.

Materials	Broken position				pH value		
	7 days		90 days				
	Intestinal tube	Anastomotic stoma	Intestinal tube	Anastomotic stoma	pH = 6	pH = 7	pH = 8
Mg-MP staples (n = 12)	0	3	4	5	4	7	1
Ti staples (n = 11)	0	3	3	5	4	6	1

3.2.2. In vivo biocompatibility

Pathological evaluations support the analysis of the local tissue response to the degradation of Mg-MP staples. Fig. 6(a) shows the representative intestine tissues surrounding Mg-MP and Ti staples stained with H&E and Masson. Holes pierced by staples are visible in images as the arrows refer to. Many infiltrating inflammatory cells are observed at two-time points, while this inflammation reaction subsides at 90 days. Moreover, abundant collagen and well-organized fibrous elastin are also observed at postoperative 90 days. As the H&E staining image in Fig. 6(b), a small number of lymphocytes are found with no neutrophils and no tissue necrosis. To further identify the inflammatory cell type, immunohistochemistry staining with several antibodies is performed. Staining with the CD3 antibody confirms the existence of T lymphocytes in two groups after 90 days, while the CD20 and CD68 antibody staining are negative. Fig. 6(c) shows the ultrastructure of intestinal epithelial cells at the anastomotic stoma after 90 days. The tight junction of epithelial cells and the goblet cells with secretion function containing rich mucus particles are normal. The uniform size microvilli of the intestinal mucosa epithelial cells are arranged neatly. There are no histopathological changes or abnormal growth.

To explore the effect of translocation and metabolism of degradation products on organs, we analyze the pathological observation and alloying elements concentration of internal organs. Fig. 7(a) shows H&E staining images and ultrastructure investigated by TEM of the heart, liver, kidney, brain, and spleen tissue. No inflammatory cell infiltration, histopathological changes, or corrosion product accumulation is observed after 90 days. The aggregation of chromatin and the number of mitochondria in hepatocytes are normal. No degeneration and necrosis are observed in glomerular capillary endothelial cells. All organs exhibit a healthy histological morphology. Fig. 7(b) depicts the concentration of magnesium, aluminum, zinc, and manganese ions in organs besides muscle and bone. By comparison with the Ti staple group, these ion

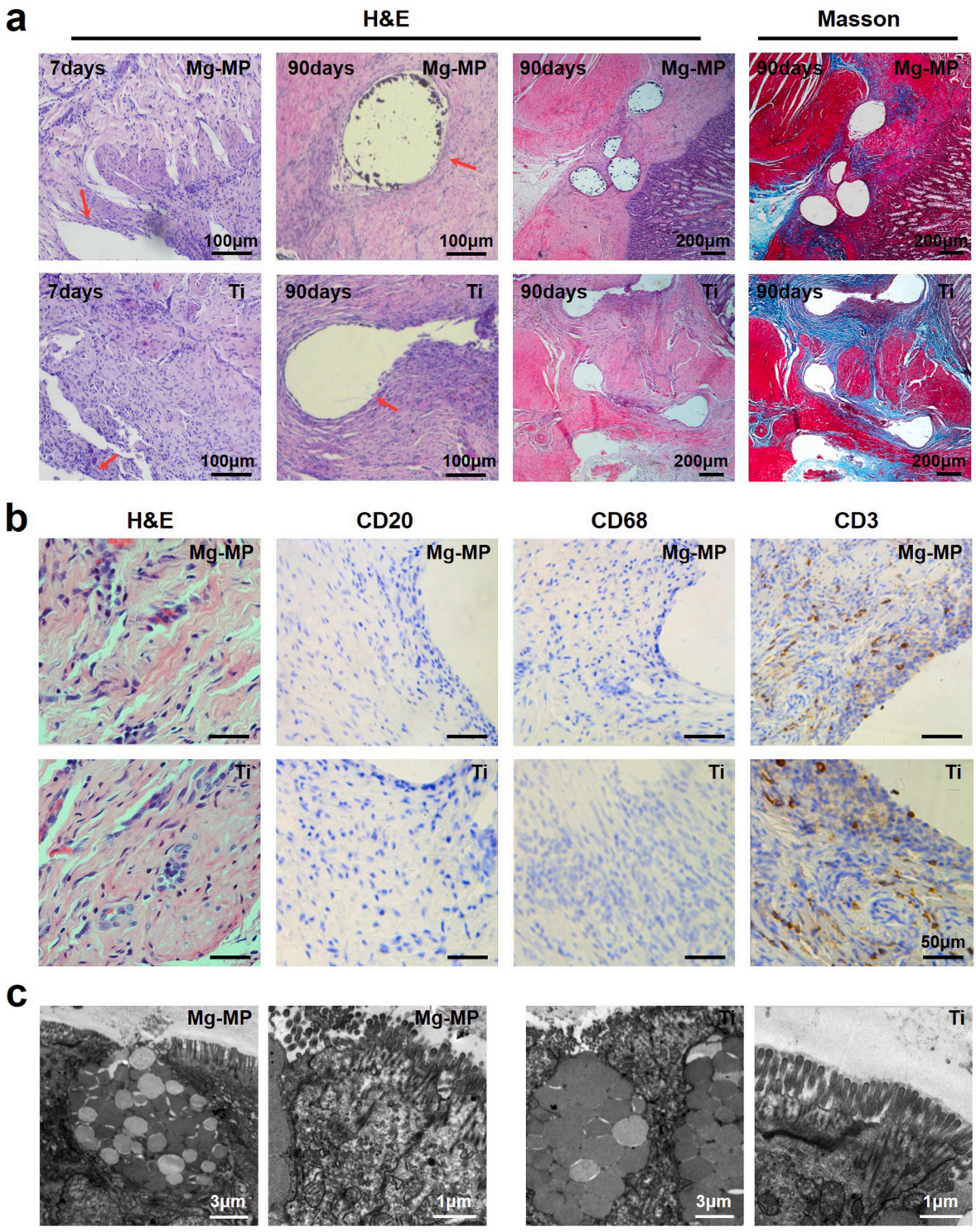

Fig. 6. Postoperative histology results of tissue surrounding the staples by (a) H&E and Masson staining (red arrow refers to the holes pierced by staples), (b) immunohistochemical staining of CD20, CD68, and CD3 antibody. The ultrastructure of intestinal epithelia around the anastomotic stoma by TEM at 90 days (c).

concentrations in the Mg-MP staple group are not statistically abnormal. There is no significant difference in both groups, which implies the degradation products of Mg-MP staples do not cause abnormal effects on the muscle, bone, and internal organs.

Dogs' peripheral blood was collected at preoperative 1 day (Pre-1) and postoperative 7, 28, and 90 days for detecting physiological indicators (Fig. 7(c)). The value of white blood cells increases significantly at 7 days but returns to normal at 28 days. The blood biochemical analysis indicates normal functions of internal organs and no statistical significance between Mg-MP staples and the control group. In contrast to the Ti staple group, the concentration of serum magnesium ion, calcium ion, and potassium ion are not disturbed with the degradation of these Mg-based staples.

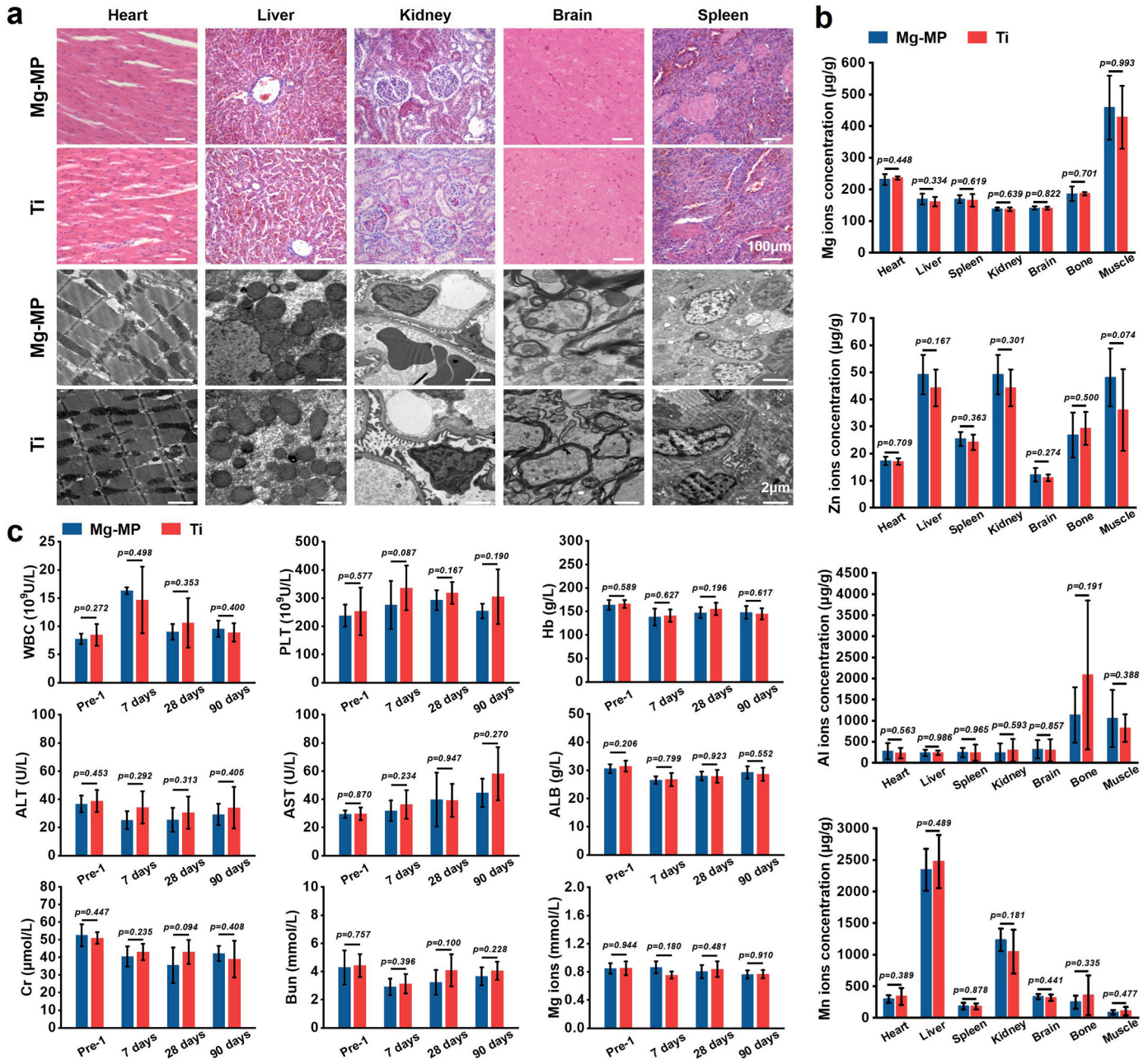

Fig. 7. Pathological images and the ultrastructure observation of the internal organs (heart, liver, kidney, brain, and spleen) at postoperative 90 days (a), and element analysis (μg/g) of alloying elements (magnesium, aluminum, zinc, and manganese ions) in organs including the muscle and bone at postoperative 90 days (b). The blood biochemical analysis of dogs' peripheral blood after implanting Mg-MP and Ti staples at each time point (preoperative 1 day, postoperative 7, 28, and 90 days).

4. Discussion

4.1. The feasibility of Mg-MP staples for colonic anastomosis

Surgical staples are used to facilitate the closure and healing of wounds by upholding tissues together. For colonic anastomosis, an ideal biodegradable anastomotic material should fulfill several fundamental criteria, including good initial corrosion resistance, adapted and lasting mechanical properties, suitable degradation rate, and good biocompatibility. In light of this, we fabricated a type of Mg-based staple with favorable mechanical properties and biodegradability and verified its feasibility to apply in colonic anastomosis.

4.1.1. In the view of staple degradation

Biocompatibility is one of the most pivotal factors to be evaluated when considering one material as a medical device. For the biodegradable materials, degradation products and ions released from devices should not induce local or systemic toxicity at least and might better help the healing process [16,31–33]. Regarding the staple we design in this study, the degradation of this staple does not cause cytotoxicity, hemolysis, or abnormal skin irritation, which illustrates its good *in vitro* biocompatibility. *In vitro* degradation tests show the degradation of Mg is largely inhibited by using the dual-layer coating. As shown in Figs. 3(f) and Fig. 4(d), the daily magnesium ions released from coated staples soaked in two ways are less than 2.5 mg and 0.05 mg, respectively, which is much less than the body's daily intake of Mg [30]. As for the *in vivo* experiment, there is no statistically significant difference in the level

of serum magnesium ion between Mg-MP and Ti groups after implantation (Fig. 7). The degradation of the Mg-MP staples does not cause an increase in serum magnesium levels. Likewise, the whole weight of aluminum in a set of Mg-MP staples is only 1.02 mg. Even though excess aluminum ions can damage nerve tissue [34], the absorbent amount from the degradation product is much less than the aluminum intake of 60 mg per day [35]. Additionally, the quantity of magnesium, aluminum, zinc, and manganese in the brain, heart, kidney, spleen, and liver also demonstrates no element accumulation after Mg-MP staples are fully biodegraded. Hepatorenal function and organ pathology examination show no abnormality during the whole implantation period. Therefore, there is no need to worry about the excessive Mg resulting from the degradation of staples.

Adequate support time during the healing process is another vital requirement for anastomotic staples. The premature failure of staples may lead to anastomotic fistula and even risk patients' life. Therefore, unlike the permanent implant material, the mechanical properties of biodegradable materials, especially their changes during degradation, catch much attention. From the result of *in vitro* bursting pressure, there is no leakage when the bursting pressure is about 3.6 kPa. All intestines are broken along the staple holes in both groups (Fig. 2(g)). Therefore, magnesium staples have sufficient support at the beginning of implantation. As obtained from the immersion result, the tension force of the Mg-MP staple can remain for 14 days, suggesting that the dual-layer coating has an effective protective effect on the Mg substrate. After the implantation of 7 days, Mg-MP staples are detected as shown in Fig. 5(a). The intestine already has a certain strength and is not entirely dependent on the support of staples at this time. Thus, the mechanical properties of magnesium alloy anastomotic staples meet the usage requirement.

4.1.2. Unique implantation environment

For clinical use, the biodegradable device should fit into the healing process of damaged tissues and be completely degraded after tissue healing. So far, biodegradable Mg alloys have been investigated for application in the orthopedic and cardiovascular fields mostly. The implants, such as cardiovascular stents and bone screws, need to stay in the body for several months or even years, which puts a high requirement on corrosion resistance. For the intestinal environment, even though the juices flow [36,37], intestine wriggling [38,39], and food friction might accelerate the corrosion rates of devices, the Mg-based anastomotic staple still possesses particular advantages in intestinal anastomosis. Firstly, it must be noted the healing time demanded after intestinal anastomosis is shorter. The fusion of the muscular layer is revealed after the intestinal anastomosis of six days [40], and anastomotic stoma has some mechanical strength after 7 days [41,42]. Thus, the duration time of sufficient mechanical support provided by staples should be more than one week. Even though the degradation rate of Mg alloys is fast, they may meet this requirement by improving their early corrosion resistance. Secondly, the anastomotic stoma is not a confined space. The hydrogen generated during degradation cannot be accumulated and result in tissue swelling before endothelialization [13]. The staples nailing on the anastomotic stoma inside the intestine might be discharged with feces after degradation. Thirdly, the degradation of Mg can achieve other biological functions. It is reported that magnesium staples can suppress inflammatory responses and promote the regeneration of tight junctions in the intestine compared to titanium [21,43]. Costantino et al. [44] also supported that the Mg-based biomaterials could induce a faster inflammation resolution while improving tissue repair. Additionally, the anti-tumor effect of magnesium degradation has also been concerned [45,46].

4.2. The degradation process of the Mg-MP staple with tissue healing

The MAO ceramic coating is an efficient surface treatment to improve the corrosion resistance of Mg alloys and adhesion strength between the polymer film with Mg substrate [25,47,48]. The composite coating of MAO and polymers has been reported in numerous previous studies [28,29,49]. Unlike preparing a coating on a metal material without subsequent deformation, coatings on the staple need to withstand the deformation when staples anastomose the intestinal wall. As shown in Fig. S8, the MAO coating is broken at the position with the large deformation, and the PLLA coating is folded inside the staple due to the pressure stress. Herein, given the *in vitro* results of staples, we summarize three main factors to explain the degradation of Mg-MP staples: (1) The PLLA coating is permeable to the solution thereby the corrosion preferentially occurs at the interface of PLLA coating and substrate, especially at the cracks on the MAO coating [29]. (2) Due to the hydrolysis and the swelling stress caused by hydrogen bubbles and the external tension, PLLA coating becomes more fragile with time [50]. The failure of PLLA coating accelerates the degradation rate of the staple, and the degradation of Mg conversely promotes the hydrolysis of polylactic acid. (3) The middle part of the staple is covered with tissues after implantation, and the surrounding tissue acts as a barrier layer to prevent staples from being corroded by flowing intestine juices. In a word, based on the degradation mechanism *in vitro* and the conditions *in vivo*, the degradation evolution of the Mg-MP staple with the healing process is shown in Fig. 8. At the initial stage of implanting, the staple tip without coatings is firstly degraded. The solution also penetrates through PLLA coating to the interface, resulting in corrosion of the substrate, especially at the deformed position exposed in the intestinal juice (Fig. 5(a), Fig. 8-II). Meanwhile, the anastomotic wound is mild swelling with many infiltrated inflammatory cells after 7-day implantation (Fig. 6(a)) and achieves primary healing. The bursting pressure of the Mg-MP group is 27.7 kPa, 74% of that after 90 days. When the generation rate of hydrogen or degradation products is more than the volume loss of substrate, PLLA coating will be peeled off under internal and external stress as shown in Fig. 8-III. At the same time, staples should have been covered with intestinal tissue. As the corrosion proceeds, the fluid is more likely to permeate from the rupture position of PLLA coating and degrade the segments wrapped in tissue, eventually causing the breakdown of staples. As a result, all the staples degrade within 90 days entirely, and the inflammation reaction also subsides. The average bursting pressure of the intestine in the Mg-MP group is about 37.4 kPa, which is no significant difference from the 35.1 kPa in the Ti group statistically. The intestinal reconstruction is completed (Fig. 8-IV). The Mg-MP staples can assume the role of Ti staples for colon reconstruction and be completely degraded without any side effects.

4.3. Outlook of this research

Table 2 lists the recent *in vivo* studies on Mg and Zn alloys in the gastrointestinal tract. Compared with Mg alloys, the zinc alloy staple with better corrosion resistance exhibits a slower degradation rate in a more hostile environment. However, its degradation time is too long for gastrointestinal healing. For Mg alloys without coatings, the degradation time of them in the gastrointestinal tract is closely related to the implantation method and material. Based on the comparison of Mg alloy ring and staple, the direct contact with gastrointestinal fluids might cause the rapid degradation of Mg alloys. Therefore, ensuring the sufficient mechanical support of Mg alloy staple during initial gastrointestinal healing is particularly important for patient safety. To sum up, biodegradable surgical staples have made some progress in recent years but still do not receive enough attention. On the one hand, the complex and diverse environment of the gastrointestinal tract requires comprehensive verification of biodegradable staples, and on the other hand, the feasibility verification of staples requires more large animal experiments. At present, the proportion of suture staples in surgery has increased year by year, especially in the application of endoscopic surgery [54]. In addition to the gastrointestinal tract, suture staples can also be widely applied for pulmonary anastomosis [55], bronchial anastomosis [56,57], and esophagogastric anastomosis [58]. Therefore, more

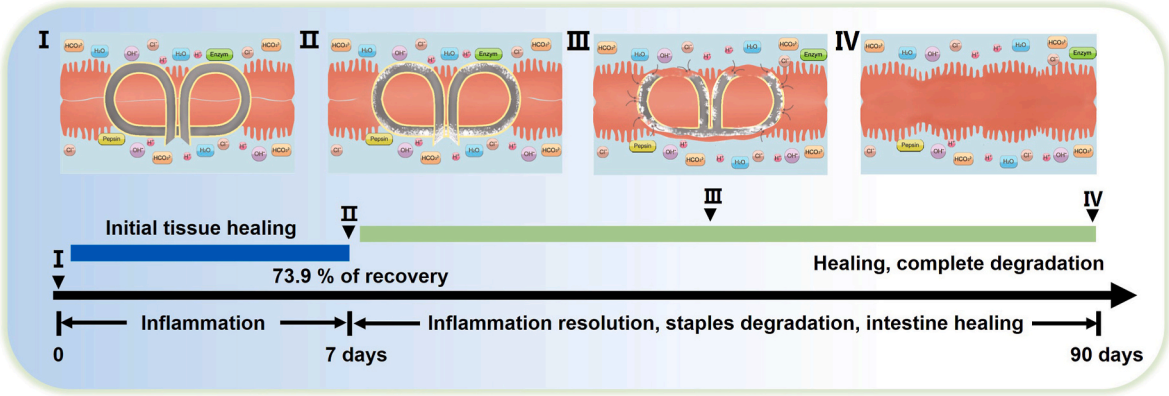

Fig. 8. Schematic diagram of the evolution of degradation mechanism of Mg-MP staple with the healing process (figure I - IV are the cross-section view of colon tissue with the staple nailed, the red part refers to the intestinal wall).

Table 2
Recent *in vivo* studies on magnesium and zinc alloys in the gastrointestinal tract [14,19,27,51–53].

Materials	Implantation methods	Duration	Final state
Mg–Zn–Y-Nd stent with MAO/PLLA coating	Implanted in the pigs' intestine	8 days	Structural integrity
Mg–4Zn-0.1Sr ring	Implanted in the pigs' small intestine	2 weeks	Broken
Mg-2Nd-1Y staple	Stapled the pigs' intestine	4 weeks	Incomplete degradation
Mg–2Zn-0.5Nd wire	Knotted on the intestine and stomach	8 weeks	Incomplete degradation
HP-Mg staple	Stapled the wall of pigs' stomach	9 weeks	Without fracture
Zn-0.8Li-0.1Mn staple	Gastrointestinal anastomosis of pigs	12weeks	89 ± 2% of the remaining volume

exploration works of biodegradable staples are still needed in the future.

Based on the research result that we had successfully prepared continuous high-performance magnesium alloy wires in 2010, we completed all animal experiments in 2012. It had been more than ten years since the current study was initiated. With the development of subsequent research, we found our trial has several limitations regarding the selection of magnesium alloy and the design of animal experiments. First, due to the lack of research on medical magnesium alloys at that time, AZ31 was basically the only alternative to successfully prepare fine wire and staples due to its excellent combination of mechanical properties and deformability. However, Al-containing magnesium alloy is not the best choice for implants. This has been improved in our subsequent studies. At present, Mg–Zn alloy wires have been successfully prepared and rival the mechanical properties of AZ31. Relevant research results regarding the microstructure, mechanical properties, and *in vitro* degradation behaviors have been reported [17,18,25,26]. Second, to obtain the statistically significant *in vivo* result, we only selected postoperative 7 days and 90 days as the test points, corresponding to the short time point that the wound was closing up and the long time point in which the staple had completely degraded. Due to budget constraints and an urgent need to explore the feasibility of the magnesium alloy surgical staple, we performed the stomach-small intestine and colon-colon anastomoses on one dog. Even with two sets of magnesium alloy staples, all dogs implanted with magnesium staples survived, and there were no statistically significant differences in all physiological indices compared with the titanium group. However, since the gastric and small intestinal environments are very complex and not conducive to the study of magnesium alloys, we reported the *in vivo* results of colonic anastomosis in this paper. Due to these limitations, systematic experimental results are not reported publicly in time. At present, more detailed work about magnesium staples is still underway, and the above deficiencies will be improved in the follow-up experiments.

5. Conclusion

In this study, we fabricated a type of full-biodegradable Mg-based surgical staple for colonic anastomosis, and the performance of this staple was evaluated using a dog model. *In vivo* experiments demonstrated that the Mg-based staple remained in its integrated structure after 7 days and completed degradation after 90 days. The degradation of Mg-based staples showed excellent biocompatibility without severe inflammation, tissue necrosis, or abnormal hyperplasia. The colon wound recovered at postoperative 90 days without leakage and stenosis. 12 dogs with Mg-based staples fully recovered with no element accumulation in organs. Considering the *in vitro* and *in vivo* results, we proposed the degradation mechanism of this staple with the situation of tissue healing. The favorable performance makes this Mg-based anastomotic staple an ideal candidate for colon reconstruction in medicine.

Ethics approval and consent to participate

In this study, we commissioned the Sanitation & Environment Technology institute of Soochow University Ltd. China. to complete the skin sensitization test and intracutaneous stimulation test. The animal experiments for the skin sensitization test and the intracutaneous stimulation test were authorized by the Laboratory Animal Center of Soochow University (License No. SCXK (Su) 2009–0005, SYXK (Su) 2007–0035). Besides, the animal experimental protocol regarding 24 beagle dogs was authorized by the medical ethics committee of Peking University People's Hospital according to the Guidance Suggestions (SYXK (Jing) 2008–0021).

CRediT authorship contribution statement

Yue Zhang: Data curation, Conceptualization, Methodology, Formal analysis, Writing – original draft. **Jian Cao:** Data curation, Investigation, Writing – review & editing, Methodology. **Mengmeng Lu:** Supervision. **Yi Shao:** Data curation, Investigation. **Kewei Jiang:** Methodology, Formal analysis. **Xiaodong Yang:** Investigation. **Xiaoyu Xiong:** Investigation. **Shan Wang:** Investigation, Formal analysis. **Chenglin Chu:** Resources, Methodology. **Feng Xue:** Conceptualization, Funding acquisition. **Yingjiang Ye:** Conceptualization, Writing – review & editing. **Jing Bai:** Conceptualization, Visualization, Funding acquisition, Writing – review & editing.

Declaration of competing interest

The authors declare no conflict of interest.

Acknowledgement

This work was supported by the National Natural Science Foundation of China (51971062, 81901056), the Natural Science Foundation of Jiangsu (BK20190649), the Science and Technology Project of Jiangsu Province (BE2019679), the Technological Innovation of key Industry of Suzhou (SYG202116), and the open research fund of Jiangsu Key Laboratory for Advanced Metallic Materials (AMM2021A01). The authors would also like to thank the Shiyanjia Lab (www.shiyanjia.com) for the ICP-OES analysis.

Appendix A. Supplementary data

Supplementary data to this article can be found online at https://doi.org/10.1016/j.bioactmat.2022.09.023.

References

[1] P.Y.G. Choy, I.P. Bissett, J.G. Docherty, B.R. Parry, A.E. H Merrie, Stapled versus handsewn methods for ileocolic anastomoses, Cochrane Db. Syst. Rev. 9 (9) (2011) CD004320. https://10.1002/14651858.CD004320.pub2.

[2] H.L. Wu, C.L. Zhao, J.H. Ni, S.X. Zhang, J.Y. Liu, J. Yan, Y.G. Chen, X.N. Zhang, Research of a novel biodegradable surgical staple made of high purity magnesium, Bioact. Mater. 1 (2) (2016) 122–126, https://doi.org/10.1016/j.bioactmat.2016.09.005.

[3] S.N. Aulestia, J.L. Leyba, S.N. Llopis, V. Pulgar, One anastomosis gastric bypass/minigastric bypass in patients with BMI<35 kg/m^2 and type 2 diabetes mellitus: preliminary report, Obes. Surg. 29 (14) (2019) 3987–3991, https://doi.org/10.1007/s11695-019-04071-4.

[4] S. Petersen, J. Jongen, W. Schwenk, Agraffectomy after low rectal stapling procedures for hemorrhoids and rectocele, Tech. Coloproctol. 15 (3) (2011) 259–264, https://doi.org/10.1007/s10151-011-0704-6.

[5] Y. Nakashima, D.H. Sun, M.C.D. Trindade, L.E. Chun, Y. Song, S.B. Goodman, D. J. Schurman, W.J. Maloney, R.L. Smith, Induction of macrophage C-C chemokine expression by titanium alloy and bone cement particles, J. Bone Joint Surg. Br. 81 (1) (1998) 155–162, https://doi.org/10.1302/0301-620X.81B1.8884.

[6] P.D. Nardi, C. Bottini, L.F. Scucchi, A. Palazzi, M. Pescatori, Proctalgia in a patient with staples retained in the puborectalis muscle after STARR operation, Tech. Coloproctol. 11 (4) (2007) 353–356, https://doi.org/10.1007/s10151-007-0381-7.

[7] Y.F. Zheng, X.N. Gu, F. Witte, Biodegradable metals, Math. Sci. Eng. R. 77 (2014) 1–34, https://doi.org/10.1016/j.mser.2014.01.001.

[8] T. Okada, T. Hayashi, Y. Ikada, Degradation of collagen suture in vitro and in vivo, Biomaterials 13 (7) (1992) 448–454, https://doi.org/10.1016/0142-9612(92)90165-K.

[9] C.E. Lang, J.M. Kremer, E.A. Berger, Organotypical engineering of differentiated composite-skin equivalents of human keratinocytes in a collagen-GAG matrix (INTEGRA Artificial Skin) in a perfusion culture system, Langenbeck Arch. Surg. 386 (5) (2001) 357–363, https://doi.org/10.1007/s004230100227.

[10] J. Nitsche, C. Howell, T. Howell, Skin closure with subcuticular absorbable staples after cesarean section is associated with decreased analgesic use, Arch. Gynecol. Obstet. 285 (4) (2012) 979–983, https://doi.org/10.1007/s00404-011-2121-5.

[11] Y. Chen, W. Zhang, M.F. Maitz, M. Chen, H. Zhang, J. Mao, Y. Zhao, N. Huang, G. Wan, Comparative corrosion behavior of Zn with Fe and Mg in the course of immersion degradation in phosphate buffered saline, Corrosion Sci. 111 (2016) 541–555, https://doi.org/10.1016/j.corsci.2016.05.039.

[12] J.Y. Fu, Y.C. Su, Y.X. Qin, Y.F. Zheng, Y.D. Wang, D.H. Zhu, Evolution of metallic cardiovascular stent materials: a comparative study among stainless steel, magnesium and zinc, Biomaterials 230 (2020), 119641, https://doi.org/10.1016/j.biomaterials.2019.119641.

[13] F. Witte, The history of biodegradable magnesium implants: a review, Acta Biomater. 6 (5) (2010) 1680–1692, https://doi.org/10.1016/j.actbio.2010.02.028.

[14] H. Guo, Z.Q. Shen, D.X. Du, Y.F. Zheng, J.R. Peng, In vitro and in vivo studies of biodegradable Zn-Li-Mn alloy staples designed for gastrointestinal anastomosis, Acta Biomater. 121 (2021) 713–723, https://doi.org/10.1016/j.actbio.2020.12.017.

[15] W.J. Lin, D.Y. Zhang, G. Zhang, H.T. Sun, H.P. Qi, L.P. Chen, Z.Q. Liu, R.L. Gao, W. Zheng, Design and characterization of a novel biocorrodible iron-based drug-eluting coronary scaffold, Mater. Des. 91 (2016) 72–79, https://doi.org/10.1016/j.matdes.2015.11.045.

[16] H.T. Yang, C. Wang, C.Q. Liu, H.W. Chen, Y.F. Wu, J.T. Han, Z.C. Jia, W.J. Lin, D. Y. Zhang, W.T. Li, W. Yuan, H. Guo, H.F. Li, G.X. Yang, D.L. Kong, D.H. Zhu, K. Takashima, L.Q. Ruan, Y.F. Zheng, Evolution of the degradation mechanism of pure zinc stent in the one-year study of rabbit abdominal aorta model, Biomaterials 145 (2017) 92–105, https://doi.org/10.1016/j.biomaterials.2017.08.022.

[17] Y. Zhang, K.Y. Chen, H. Liu, Y. Shao, C.L. Chu, F. Xue, J. Bai, A study of a biodegradable braided Mg stent for biliary reconstruction, J. Mater. Sci. 55 (2020) 17170–17182, https://doi.org/10.1007/s10853-020-05289-9.

[18] Y. Zhang, J. Cao, X.L. Wang, H. Liu, Y. Shao, C.L. Chu, F. Xue, J. Bai, The effect of enzymes on the in vitro degradation behavior of Mg alloy wires in simulated gastric fluid and intestinal fluid, Bioact. Mater. 7 (2021) 217–226, https://doi.org/10.1016/j.bioactmat.2021.05.047.

[19] Q.L. Huang, L. Liu, H. Wu, K.M. Li, N.F. Li, Y. Liu, The design, development, and in vivo performance of intestinal anastomosis ring fabricated by magnesium-zinc-strontium alloy, Mat. Sci. Eng. C-Mater. 106 (2020), 110158, https://doi.org/10.1016/j.msec.2019.110158.

[20] J. Yan, Y.G. Chen, Q.L. Yuan, X.H. Wang, S. Yu, W.C. Qiu, Z.G. Wang, K.X. Ai, X. N. Zhang, S.X. Zhang, C.L. Zhao, Q. Zheng, Comparison of the effects of Mg–6Zn and Ti–3Al–2.5V alloys on TGF-β/TNF-α/VEGF/b-FGF in the healing of the intestinal tract in vivo, Biomed. Mater. 9 (2) (2014), 025011, https://doi.org/10.1088/1748-6041/9/2/025011.

[21] J.Z. Xia, H. Chen, J. Yan, H.L. Wu, H. Wang, J. Guo, X.N. Zhang, S.X. Zhang, C. L. Zhao, Y.G. Chen, High-Purity magnesium staples suppress inflammatory response in rectal anastomoses, ACS Appl. Mater. Interfaces 9 (2017) 9506–9515, https://doi.org/10.1021/acsami.7b00813.

[22] J. Yan, Y.G. Chen, Q.L. Yuan, S. Yu, W.C. Qiu, C.G. Yang, Z.G. Wang, J.F. Gong, K. X. Ai, Q. Zheng, J.N. Li, S.X. Zhang, X.N. Zhang, Comparison of the effects of Mg–6Zn and titanium on intestinal tract in vivo, J. Mater. Sci. Mater. Med. 24 (6) (2013) 1515–1525.

[23] X. Li, C. Shi, J. Bai, C. Guo, F. Xue, P.H. Lin, C.L. Chu, Degradation behaviors of surface modified magnesium alloy wires in different simulated physiological environments, Front. Mater. Sci. 8 (3) (2014) 281–294, https://doi.org/10.1007/s11706-014-0257-5.

[24] X. Lin, L.L. Tan, Q. Zhang, K. Yang, Z.Q. Hu, J.H. Qiu, Y. Cai, The in vitro degradation process and biocompatibility of a ZK60 magnesium alloy with a forsterite-containing micro-arc oxidation coating, Acta Biomater. 9 (10) (2013) 8631–8642, https://doi.org/10.1016/j.actbio.2012.12.016.

[25] H. Cai, Y. Zhang, J. Meng, X. Li, F. Xue, C.L. Chu, L. Tao, J. Bai, Enhanced fully-biodegradable Mg&PLA composite rod: effect of surface modification of Mg-2Zn wire on the interfacial bonding, Surf. Coating. Technol. 350 (2018) 722–731, https://doi.org/10.1016/j.surfcoat.2018.07.045.

[26] L.X. Sun, J. Bai, F. Xue, L. Tao, C.L. Chu, J. Meng, Exceptional texture evolution induced by multi-pass cold drawing of magnesium alloy, Mater. Des. 135 (2017) 267–274, https://doi.org/10.1016/j.matdes.2017.09.027.

[27] M. Gao, D. Na, X.Q. Ni, L.H. Song, I.P. Etim, K. Yang, L.L. Tan, Z. Ma, The mechanical property and corrosion resistance of Mg-Zn-Nd alloy fine wires in vitro and in vivo, Bioact. Mater. 6 (1) (2021) 55–63, https://doi.org/10.1016/j.bioactmat.2020.07.011.

[28] P. Shi, B. Niu, S.S. E, Y. Chen, Q. Li, Preparation and characterization of PLA coating and PLA/MAO composite coatings on AZ31 magnesium alloy for improvement of corrosion resistance, Surf. Coating. Technol. 262 (2015) 26–32, https://doi.org/10.1016/j.surfcoat.2014.11.069.

[29] R.C. Zeng, L.Y. Cui, K. Jiang, R. Liu, B.D. Zhao, Y.F. Zheng, In vitro corrosion and cytocompatibility of a microarc oxidation coating and poly(l-lactic acid) composite coating on Mg–1Li–1Ca alloy for orthopedic implants, ACS Appl. Mater. Interfaces 8 (15) (2016) 10014–10028, https://doi.org/10.1021/acsami.6b00527.

[30] F.I. Wolf, A. Cittadini, Chemistry and biochemistry of magnesium, Mol. Aspect. Med. 24 (1) (2003) 3–9, https://doi.org/10.1016/S0098-2997(02)00087-0.

[31] Y.M. Tang, S.H. Lin, S. Yin, F. Jiang, M.L. Zhou, G.Z. Yang, N.J. Sun, W.J. Zhang, X. Q. Jiang, In situ gas foaming based on magnesium particle degradation: a novel approach to fabricate injectable macroporous hydrogels, Biomaterials 232 (2020), 119727, https://doi.org/10.1016/j.biomaterials.2019.119727.

[32] Y. Li, J.K. Xu, J. Mi, X. He, Q. Pan, L.Z. Zheng, H.Y. Zu, Z.Y. Chen, B.Y. Dai, X. Li, Q. Q. Pang, L. Zhou, L. Huang, W.X. Tong, G. Li, L. Qin, Biodegradable magnesium combined with distraction osteogenesis synergistically stimulates bone tissue regeneration via CGRP-FAK-VEGF signaling axis, Biomaterials 275 (2021), 120984, https://doi.org/10.1016/j.biomaterials.2021.120984.

[33] J.L. Wang, J.K. Xu, C. Hopkins, D.H.K. Chow, L. Qin, Biodegradable magnesium - based implants in orthopedics - a general review and perspectives, Adv. Sci. 7 (8) (2020), 1902443, https://doi.org/10.1002/advs.201902443.

[34] C. Rössig, N. Angrisani, P. Helmecke, S. Besdo, J.M. Seitz, B. Welke, N. Fedchenko, H. Kock, J. Reifenrath, In vivo evaluation of a magnesium-based degradable intramedullary nailing system in a sheep model, Acta Biomater. 25 (2015) 369–383, https://doi.org/10.1016/j.actbio.2015.07.025.

[35] M.C. Zhao, M. Liu, G.L. Song, A. Atrens, Influence of pH and chloride ion concentration on the corrosion of Mg alloy ZE41, Corrosion Sci. 50 (11) (2008) 3168–3178, https://doi.org/10.1016/j.corsci.2008.08.023.

[36] J. Wang, V. Giridharan, V. Shanow, Z.G. Xu, B. Collins, L. White, Y. Jang, J. Sankar, N. Huang, Y. Yun, Flow-induced corrosion behavior of absorbable magnesium-based stents, Acta Biomater. 10 (2014) 5213–5223, https://doi.org/10.1016/j.actbio.2014.08.034.

[37] L.Y. Han, X. Li, F. Xue, C.L. Chu, J. Bai, Biocorrosion behavior of micro-arc-oxidized AZ31 magnesium alloy in different simulated dynamic physiological environments, Surf. Coating. Technol. 361 (2019) 240–248, https://doi.org/10.1016/j.surfcoat.2019.01.052.

[38] L.Y. Han, Z.W. Zhang, J.W. Dai, X. Li, J. Bai, Z.H. Huang, C. Guo, F. Xue, C.L. Chu, The influence of alternating cyclic dynamic loads with different low frequencies on the bio-corrosion behaviors of AZ31B magnesium alloy in vitro, Bioact. Mater. 7 (2022) 263–274, https://doi.org/10.1016/j.bioactmat.2021.05.049.

[39] R.L. Wilson, C.E. Stevenson, Chapter 56 - anatomy and physiology of the stomach, in: C.J. YEO (Ed.), Shackelford's Surgery of the Alimentary Tract, Elsevier Inc.

Philadelphia, 2019, pp. 634–646, https://doi.org/10.1016/B978-0-323-40232-3.00056-X.
[40] I. Kott, M. Lurie, The effects of electrosurgery and the surgical knife on the healing of intestinal anastomoses, Dis. Colon Rectum 16 (1) (1973) 33–38, https://doi.org/10.1007/BF02589907.
[41] C.A. Bundy, D.M. Jacobs, R.T. Zera, M.P. Bubrick, Comparison of bursting pressure of sutured, stapled and BAR anastomoses, Int. J. Colorectal Dis. 8 (1) (1993) 1–3, https://doi.org/10.1007/BF00341267.
[42] T. Hendriks, W.J.B. Mastboom, Healing of experimental intestinal anastomoses, Dis. Colon Rectum 33 (10) (1990) 891–901, https://doi.org/10.1007/bf02051930.
[43] S. Yu, X.H. Wang, Y.G. Chen, Q. Zheng, X.N. Zhang, C.L. Zhao, S.X. Zhang, J. Yan, In vitro and in vivo evaluation of effects of Mg–6Zn alloy on tight junction of intestinal epithelial cell, T. Nonferr. Metal. Soc. 25 (11) (2015) 3760–3766, https://doi.org/10.1016/S1003-6326(15)64014-6.
[44] M.D. Costantino, A. Schuster, H. Helmholz, A. Meyer-Rachner, R. Willumeit-Römer, B.J.C. Luthringer-Feyerabend, Inflammatory response to magnesium-based biodegradable implant materials, Acta Biomater. 101 (2020) 598–608, https://doi.org/10.1016/j.actbio.2019.10.014.
[45] J. Long, W. Zhang, Y.Q. Chen, B. Teng, B. Liu, H.L. Li, Z.Y. Yao, D. Wang, L. Li, X. F. Yu, L. Qin, Y.X. Lai, Multifunctional magnesium incorporated scaffolds by 3D-Printing for comprehensive postsurgical management of osteosarcoma, Biomaterials 275 (2021), 120950, https://doi.org/10.1016/j.biomaterials.2021.120950.
[46] H.Z. Peng, K. Fan, R. Zan, Z.J. Gong, W.T. Sun, Y. Sun, W.H. Wang, H.M. Jiang, J. Lou, J.H. Ni, T. Suo, X.N. Zhang, Degradable magnesium implants inhibit gallbladder cancer, Acta Biomater. 128 (2021) 514–522, https://doi.org/10.1016/j.actbio.2021.04.051.
[47] X. Lin, L.L. Tan, Q. Zhang, K. Yang, Z.Q. Hu, J.H. Qiu, Y. Cai, The in vitro degradation process and biocompatibility of a ZK60 magnesium alloy with a forsterite-containing micro-arc oxidation coating, Acta Biomater. 9 (10) (2013) 8631–8642, https://doi.org/10.1016/j.actbio.2012.12.016.
[48] W. Yang, D.P. Xu, J.L. Wang, X.F. Yao, J. Chen, Microstructure and corrosion resistance of micro arc oxidation plus electrostatic powder spraying composite coating on magnesium alloy, Corrosion Sci. 136 (2018) 174–179, https://doi.org/10.1016/j.corsci.2018.03.004.
[49] L. Xu, A. Yamamoto, In vitro degradation of biodegradable polymer-coated magnesium under cell culture condition, Appl. Surf. Sci. 258 (17) (2012) 6353–6358, https://doi.org/10.1016/j.apsusc.2012.03.036.
[50] X. Li, C.L. Chu, Y.L. Wei, C.X. Qi, J. Bai, C. Guo, F. Xue, P.H. Lin, P.K. Chu, In vitro degradation kinetics of pure PLA and Mg&PLA composite: effects of immersion temperature and compression stress, Acta Biomater. 48 (2017) 468–478, https://doi.org/10.1016/j.actbio.2016.11.001.
[51] Z.H. Wang, Q.X. Zheng, S.K. Guan, Z.B. Sun, S.P. Liu, B.B. Zhang, T.H. Duan, K. Xu, In vitro and in vivo assessment of the biocompatibility of an paclitaxel- eluting poly- L -lactide-coated Mg-Zn-Y-Nd alloy stent in the intestine, Mat. Sci. Eng. C-Mater. 105 (2019), 110087, https://doi.org/10.1016/j.msec.2019.110087.
[52] H. Amano, K. Hanada, A. Hinoki, T. Tainaka, C. Shirota, W. Sumida, K. Yokota, N. Murase, K. Oshima, K. Chiba, Y. Tanaka, H. Uchida, Biodegradable surgical staple composed of magnesium alloy, Sci Rep-UK 9 (2019), 14671, https://doi.org/10.1038/s41598-019-51123-x.
[53] S. Qu, J.Z. Xia, J. Yan, H.L. Wu, H. Wang, Y. Yi, X.N. Zhang, S.X. Zhang, C.L. Zhao, Y.G. Chen, In vivo and in vitro assessment of the biocompatibility and degradation of high-purity Mg anastomotic staples, J. Biomater. Appl. 31 (8) (2017) 1203–1214, https://doi.org/10.1177/0885328217692948.
[54] J.C. Huhn, Chapter 11 - stapling and energy devices for endoscopic surgery, in: T. R. Tams (Ed.), Small Animal Endoscopy, third ed., Elsevier Inc., 2011, pp. 363–372, https://doi.org/10.1016/B978-0-323-05578-9.10011-7.
[55] N. Matsutani, E. Kanai, R. Hanawa, Y. Takahashi, H. Uehara, H. Linuma, M. Kawamura, Pericardial conduit for pulmonary artery reconstruction by surgical stapling, Ann. Thorac. Surg. 103 (5) (2017) e469–e471, https://doi.org/10.1016/j.athoracsur.2016.11.073.
[56] M. Zakkar, R. Kanagasabay, I. Hunt, No evidence that manual closure of the bronchial stump has a lower failure rate than mechanical stapler closure following anatomical lung resection, Interact. Cardiov. Th. 18 (2014) 488, https://doi.org/10.1093/icvts/ivt502.
[57] J. Vannucci, G.L. Gervasi, M. Freddolini, A. Pistilli, V.D. Monte, A. Bufalari, M. Rende, F. Puma, Pericardium matrix buttressing hinders the stapled bronchial stump healing, J. Surg. Res. 201 (2) (2016) 286–292, https://doi.org/10.1016/j.jss.2015.11.013.
[58] P.K. Mishra, H. Shah, N. Cupta, V. Varshney, N.S. Patil, A. Jain, S.S. Saluja, Stapled versus hand-sewn cervical esophagogastric anastomosis in patients undergoing esophagectomy: a Retrospective Cohort Study, Ann. Med. Surg. 5 (2016) 118–124, https://doi.org/10.1016/j.amsu.2015.12.063.